Oxygen Diffusion Modeling in Diesel Particulate Filter Regeneration

O. A. Haralampous and G. C. Koltsakis
Laboratory of Applied Thermodynamics, Aristotle University Thessaloniki, Thessaloniki, Greece

DOI 10.1002/aic.10181
Published online in Wiley InterScience (www.interscience.wiley.com).

This study introduces a coupled reaction–diffusion model able to account for O_2 diffusion in the wall flow honeycomb particulate filter. The diffusion model is incorporated on a previously published single-channel model for the calculation of flow distribution, heat transfer, and soot oxidation reaction. A computational study is carried out aiming at evaluating the importance of O_2 diffusion effects as the function of operating conditions similar to those encountered in the real world. During controlled regeneration conditions, the effect of oxygen diffusion is minor and observable only at high soot loadings. On the other hand, the role of oxygen diffusion is shown to be critical in uncontrolled regeneration conditions, which are important for filter thermal failure. Traditional models neglecting diffusion effects are shown to strongly underpredict the maximum temperatures during uncontrolled regeneration with moderate to high soot loadings. © 2004 American Institute of Chemical Engineers *AIChE J,* 50: 2008–2019, 2004
Keywords: diesel particulate filters, regeneration, modeling, diffusion

Introduction

The diesel particulate filter (DPF) technology is nowadays recognized as a technically feasible solution for the emission control of diesel engines (Johnson, 2003). The wall-flow ceramic honeycomb particulate filter, already introduced more than 20 years ago (Abthoff et al., 1985; Howitt and Montierth, 1981), is currently the most mature filter type. This type of filters exhibits excellent filtration efficiency (>95%). The main issue associated with their application is the accumulation of soot in the filter channels, which may increase the exhaust backpressure to unacceptable levels. The filter regeneration by thermal soot oxidation is still the most challenging aspect of this technology. Because of the relatively low temperatures of the diesel exhaust gas, catalytic assistance in the form of fuel-borne catalysts (Salvat et al., 2000) or catalytic filter coatings (Suresh et al., 2001) is currently the state of the art for commercial systems. NO_2-based low-temperature soot combustion [CRT technology is the primary commercial technology for heavy-duty diesel applications (Cooper and Thoss, 1989)]. In any case, the regeneration system is largely supported by the diesel engine injection and control systems, which are responsible for increasing the exhaust gas temperature by "postinjection," thus initiating the regeneration process.

A main issue for the durability of DPF systems is their sustainability during uncontrolled regenerations, during which severe thermal gradients may lead to filter cracks or even melting. The development of critical thermal gradients depends on a large number of interrelated operating and design parameters. In this respect, mathematical modeling of the regeneration process is commonly used as a predictive tool toward system optimization.

According to the underlying assumptions, the various published models are categorized as zero-, one-, or two-dimensional. A classical zero-dimensional model was presented by Bissett and Shadman (1985). The main assumptions of the zero-dimensional approach can be summarized as follows:

(1) All channels behave in an exactly identical way, which is true, provided that the heat losses are negligible and flow at the filter face is radially uniform.

(2) The exhaust gas flows through two layers: the particle deposit, which shrinks uniformly with time during regenera-

Correspondence concerning this article should be addressed to G. C. Koltsakis at greg@antiopi.meng.auth.gr.

tion, and the porous ceramic channel wall. The soot deposition is assumed uniform over the monolith channels.

(3) The weakest assumption is probably that of equal exhaust gas temperature entering the deposit layer over the channel length. This simplifying model construction uses a single spatial variable x along the gas flow through the layers, whereas all variations in the direction perpendicular to x are neglected.

(4) The soot and wall temperatures along the x-direction are assumed uniform.

The one-dimensional (1-D) approach initially presented by Bissett (1983) raised assumption 3 (uniform exhaust gas conditions flowing through the soot layer and wall), by including the flow and heat transfer phenomena along the channel. This approach inherently allows the cancellation of assumption 2, given that the soot layer need not be uniform and is computed as a function of the distance from the filter inlet. This 1-D model is thus capable of computing the flow distribution through the wall as well as the axial temperature gradients in the gas and solid phases along a representative filter channel (Koltsakis and Stamatelos, 1997). Assumption 1 (identical behavior of all channels) is also raised in more comprehensive 2-D models, which take into account the heat losses and flow maldistribution (Aoki et al., 1993; Haralampous et al., 2003; Konstandopoulos et al., 2001; Miyairi et al., 2001). Three-dimensional models aimed at more detailed temperature and thermal stress predictions have also been published (Pontikakis et al., 2002).

Assumption 4 was also reexamined by Haralampous and Koltsakis (2002), who studied the intralayer temperature gradients expected in the soot and wall layers, in the light of recent findings regarding the microstructural particulate deposit properties.

In all previously published models, the molecular diffusion of oxygen was not taken into account. Therefore, the oxygen concentration of the exhaust in the inlet channel was considered constant and equal to that of the inflowing gas. However, oxygen diffusion may occur within the filter because of the concentration gradients developed between oxygen-rich regions of the flowing gas and oxygen-poor regions in the reacting soot layer during regeneration. This article will deal with the study of these diffusion phenomena during regeneration. The study is based on the mathematical formulation of the respective governing equations. The resulting reaction–diffusion problem will be solved for representative regeneration conditions. For simplification and more clear illustration of the oxygen diffusion effects, the modeling study will be based on a single-channel approach.

Single-Channel Model

Gas-phase flow and temperature distribution

The calculation of the flow and temperature field in the single-channel model is based on the solution of the mass, momentum, and energy balance equations. The side and front views of a channel model is given in Figure 1. The governing equations for the conservation of mass, momentum, and energy are given below:

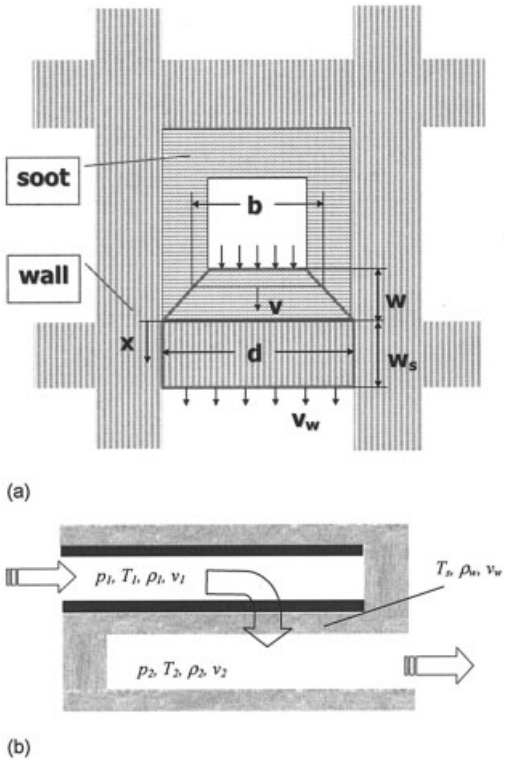

Figure 1. Channel model.

(a) Front view, (b) side view.

Conservation of Mass of Channel Gas

$$\frac{\partial}{\partial z}(d_i^2 \rho_i v_i) = (-1)^i 4 d \rho_w v_w \tag{1}$$

Conservation of the z-Component of Momentum of Channel Gas

$$\frac{\partial p_i}{\partial z} + \frac{\partial}{\partial z}(\rho_i v_i^2) = -\alpha \mu v_i / d_i^2 \tag{2}$$

Conservation of Energy of Channel Gas

(1) Inlet channel

$$C_{p,g} \rho_1 v_1 \frac{\partial T_1}{\partial z} = h_1 \frac{4}{d_1}(T_s - T_1) \tag{3}$$

(2) Outlet channel

$$C_{p,g} \rho_2 v_2 \frac{\partial T_2}{\partial z} = (h_2 + C_{p,g} \rho_w v_w) \frac{4}{d}(T_s - T_2) \tag{4}$$

Pressure Drop across the Deposit Layer and Ceramic Wall. The pressure difference across the inlet and exit channel at a fixed z is the sum of the pressure loss attributed to the flow through the soot layer and wall

$$p_1 - p_2 = \Delta p_{soot} + \Delta p_{wall} \tag{5}$$

Based on the analysis presented in Haralampous et al. (2004), the pressure loss through the soot layer is

$$\Delta p_{soot} = \frac{\Re T}{M_g \bar{p}} \frac{\mu d \rho_w v_w}{2k_p(\bar{p})} \ln\left(\frac{d}{d-2w}\right) \tag{6}$$

The soot permeability is a function of the local mean free path length and can be expressed as (Pulkrabek and Ibele,1987)

$$k_p = k_0\left(1 + C_4 \frac{p_0}{p} \mu \sqrt{\frac{T}{M_g}}\right) \tag{7}$$

The pressure loss through the porous filter wall can be described by the Darcy law

$$\Delta p_{wall} = \frac{\mu v_w}{k_s} w_s \tag{8}$$

The parameters characterizing the permeability of the soot layer k_0 and C_4 can be calibrated by engine experiments at various soot loadings, flow rates, and temperatures as described in a previous publication (Haralampous et al., 2003).

A set of boundary conditions is necessary to solve the system of differential Eqs. 1–5. The mass-flow rate and the gas temperature are given at the entrance of the inlet channel and additionally the pressure at the outlet channel exit. The solution of the system yields

- The channel flow field (v_w, v_1, v_2)
- The pressure field (p_1, p_2)
- The gas temperature field (T_1, T_2)

Based on these results, we can calculate the input parameters for the following steps of the computational procedure, such as the channel pressure drop, the heat convection in the inlet and outlet channels, and the heat convection attributed to the flow through the wall.

The output of the solution of the channel model constitutes, among other entities, the energy release along the channel. This is actually a local heat source term, which can be fed in a transient 1-D heat-transfer model of the filter to compute the temperature field in the filter.

Heat sources

Soot Oxidation Exotherm. For the calculation of heat sources, the specific filtration area of the filter s_F is defined according to the following equation

$$s_F = 2d1550 \text{ cpsi} \tag{9}$$

$$H_{react} = s_F \int_{-w}^{w_s} f_x R_1 \Delta H_1 dx \tag{10}$$

Convection of Heat Attributed to Flow through Wall

$$H_{wall} = \rho_w v_w s_F C_{p,g}(T_1 - T_s) \tag{11}$$

Convection of Heat Attributed to Flow in Channel. The convective heat-transfer coefficients are computed using the well-established relations for laminar flow convection inside a channel. The heat convection can be determined by the following equation

$$H_{conv} = h_1 s_F(T_1 - T_s) + h_2 s_F(T_2 - T_s) \tag{12}$$

Radiation Heat Transfer. During regeneration high temperatures could be developed, as well as significant axial temperature gradients. In this case, radiative heat exchange in the channels may become important. The model is equipped with a radiation heat transfer submodel, in which black body behavior of the wall surface is assumed (diesel soot is accurately approximated by a black body). Radiation exchange is calculated within each channel between different axial points, based on the view factor F

$$H_{rad} = s_F \sigma \left(T_s^4 - \frac{\int_{channel} T_s^4 F dA}{A_{channel}}\right) \tag{13}$$

The radiation term accounts for radiation exchange between the channel surface, the plug, and the opening of the channel. The radiation calculation covers both the input and output channels.

Wall temperature calculation

An explicit finite-difference method is used to solve the 1-D transient heat-transfer problem in the filter. The effective heat conductivity is calculated for the axial conduction, taking into account the respective void fraction. The properties of the exhaust gas and the filter material are calculated as functions of temperature. The temperature field in the filter is then described by the equation of transient 1-D heat conduction with heat sources

$$\rho_s C_{p,s} \frac{\partial T_s}{\partial t} = \lambda_{s,z} \frac{\partial^2 T_s}{\partial z^2} + S \tag{14}$$

The source term S includes the contribution of the convective heat transfer of the gas flow in the channels and through the wall, the exothermic heat release, and any radiated heat

$$S = H_{conv} + H_{wall} + H_{react} + H_{rad} \tag{15}$$

Adiabatic boundary conditions for the heat conduction equation are used at $z = 0, L$.

Intralayer reaction model

As shown in a previous publication (Haralampous and Koltsakis, 2002), intralayer temperature gradients in the x-direction (Figure 1a) are expected only under conditions of very high soot loading and very high flow rates. During typical operating conditions for diesel exhaust, temperatures of the soot layer and the filter wall are expected to be uniform. Therefore, herein we will confine our interest to intralayer concentration rather

Table 1. Geometry and Thermophysical Properties of the DPF Used in the Simulations

Filter Material	Cordierite
Cell density	300 cells/in.^{2} (46.5 cells/cm^2)
Wall thickness	0.356 mm
Diameter	144 mm
Length	152 mm
Plug length	10 mm
Wall density	1100 kg/m^3
Wall permeability	1.2×10^{-12}m^2
Porosity	60%
Mean pore size	25 μm

than temperature gradients. Based on the assumption of uniform temperature in the soot layer, it is straightforward to formulate an overall oxygen balance and solve for the rate of soot reaction, assuming a first-order reaction of soot with oxygen (Bissett and Shadman, 1985).

The following global reaction is considered to take place in the soot layer

$$C + \alpha_1 O_2 \rightarrow 2\left(\alpha_1 - \frac{1}{2}\right)CO_2 + 2(1 - \alpha_1)CO$$

$$R_1 = \frac{s\rho_p A_1 e^{-E_1/RT} p_{O_2}}{M_C} \tag{16}$$

where α_1 is used in the above reaction as an index of the completeness of carbon oxidation.

At high regeneration temperatures (>550°C) the formation of NO_2 is not favored because of chemical equilibrium. In this case, its contribution for carbon oxidation is neglected.

Oxygen diffusion

The consumption of O_2 in the soot layer induces a concentration gradient of O_2 between the bulk gas flow in the channels and the soot layer. Herein, we introduce an O_2 diffusion model between the gas and the soot layer, to check its importance at different regeneration conditions. The model equations of the coupled reaction–diffusion model are given below.

The governing equation for oxygen conservation in the soot layer and wall is

$$v_w \frac{\partial y}{\partial x} - D \frac{\partial}{\partial x}\left(f_x \frac{\partial y}{\partial x}\right) = \frac{f_x}{c_m} a_1 R_1 \tag{17}$$

where the geometrical parameter f_x is defined as

$$f_x = \frac{b(x)}{d} \tag{18}$$

The width available to flow $b(x)$ varies in the particulate layer and remains constant in the wall

$$b(x) = \begin{cases} d + 2x, & -w \le x < 0 \\ d, & 0 \le x \le w_s \end{cases} \tag{19}$$

The effective diffusivity is calculated based on the mixed diffusion model

$$\frac{1}{D} = \frac{\tau}{\varepsilon_p}\left(\frac{1}{D_{mol}} + \frac{1}{D_{knud}}\right) \tag{20}$$

with the Knudsen diffusivity

$$D_{knud} = \frac{d_p}{3}\sqrt{\frac{8\Re T}{\pi M_{O_2}}} \tag{21}$$

The values of porosity ϵ_p, tortuosity τ, and mean pore size d_p are based on the microstructural properties of the soot layer and the filter wall.

It has to be noted that the experimental determination of tortuosity in the soot layer and the porous wall is not straightforward, especially in porous media with nonuniform pore distribution. Different techniques facing this issue are discussed in recent work of Kolaczkowski (2003), dealing with measurements of effective diffusivity in catalyst-coated monoliths. In the case of catalytic coatings in flowthrough catalysts,

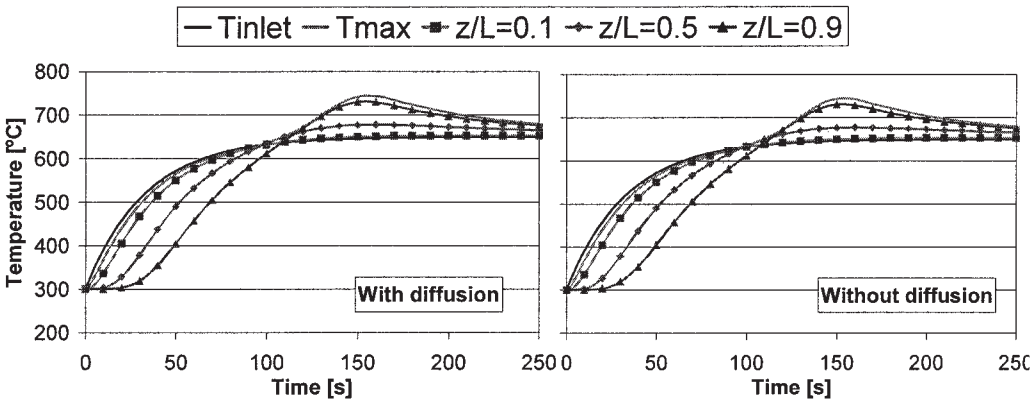

Figure 2. Comparison of temperature predictions during controlled regeneration with (left) and without O_2 diffusion (right).

Computed temperatures along the filter for 6 kg/m^{3}initial soot loading.

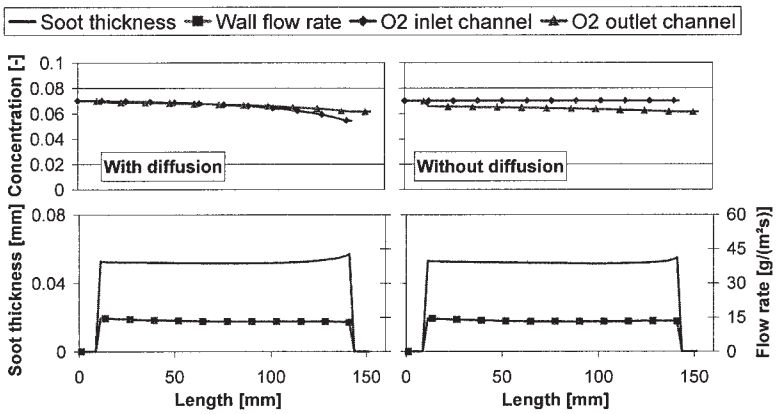

Figure 3. Profiles of O_2 concentration in the inlet and outlet channels during controlled regeneration.

Conditions: 6 kg/m^3 initial soot mass at $t = 132$ s. Also shown is the wall flow velocity and the soot layer thickness at the same time.

typical values for the tortuosity factor range from 1 to 10 (Hayes et al., 2000). In the present work, we use a value of 3.

The boundary conditions should "couple" the phenomena in the wall with the gas conditions in the inlet and outlet channels. In these boundaries, one should consider the convective mass transfer from the bulk gas to the wall surface, which can be computed as usual based on the "film" approach with mass transfer coefficients k_i corresponding to laminar flow of both inlet and outlet channels

$$\frac{\partial}{\partial z}(v_1 y_1) = -\frac{1}{df_{-w}^2} v_w y_1 + \frac{1}{df_{-w}} k_1 (y_{1s} - y_1) \tag{22}$$

$$\frac{\partial}{\partial z}(v_2 y_2) = \frac{1}{df_{w_s}^2} v_w y_{2s} + \frac{1}{df_{w_s}} k_2 (y_{2s} - y_2) \tag{23}$$

The mass-transfer coefficient for each channel is

$$k_i = \frac{\mathrm{Sh}\, D}{d_i} \tag{24}$$

The molecular flow at the surface of the deposit layer can also be expressed as

$$v_w y_{1s} - Df_{-w} \left.\frac{\partial y}{\partial x}\right|_{1s} = -df_{-w}^2 \frac{\partial}{\partial z}(v_1 y_1) \tag{25}$$

The molecular flow at the wall surface in the outlet channel is expressed as

$$v_w y_{2s} - Df_{w_s} \left.\frac{\partial y}{\partial x}\right|_{2s} = df_{w_s}^2 \frac{\partial}{\partial z}(v_2 y_2) \tag{26}$$

Combining Eqs. 22 and 25 yields the boundary condition for the inlet channel

$$v_w y_{1s} - Df_{-w} \left.\frac{\partial y}{\partial x}\right|_{1s} = v_w y_1 - k_1 f_{-w} (y_{1s} - y_1) \tag{27}$$

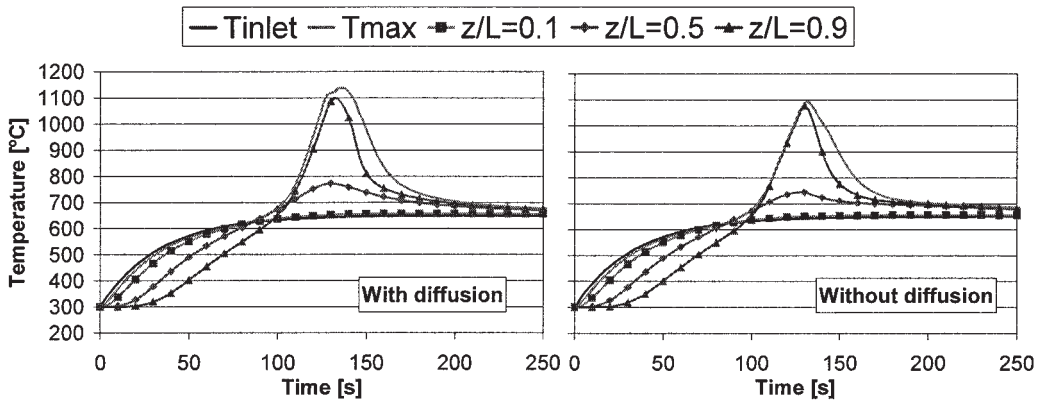

Figure 4. Comparison of temperature predictions during controlled regeneration with (left) and without O_2 diffusion (right).

Computed temperatures along the filter for 12 kg/m^3 initial soot mass.

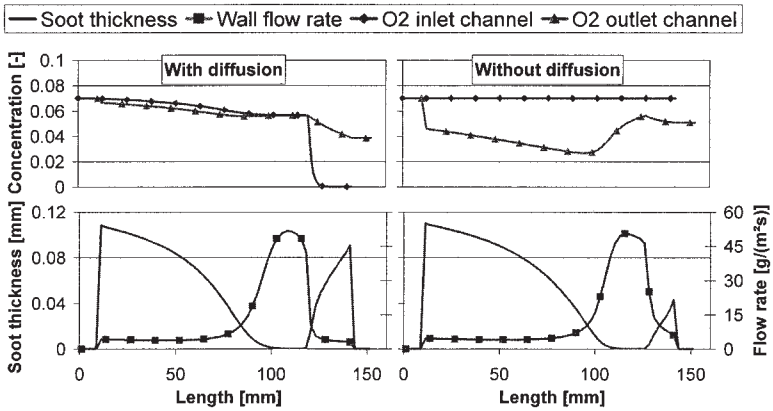

Figure 5. Profiles of O_2 concentration, in the inlet and outlet channels during controlled regeneration.

Conditions: 12 kg/m^3 initial soot mass at $t = 132$ s. Also shown is the wall flow velocity and the soot layer thickness at the same time.

Similarly Eqs. 26 and 23 yield the boundary condition for the outlet channel

$$-Df_{w_s}\left.\frac{\partial y}{\partial x}\right|_{2s} = k_2(y_{2s} - y_2) \tag{28}$$

Equations 27 and 28 are equivalent with the Danckwerts boundary conditions extended with an additional term for diffusive mass transfer with the bulk gas flowing parallel to the wall. The addition of this term implies that the concentration in the channels can vary axially.

Soot mass balance

The rate of soot mass change resulting from the reaction is

$$\frac{1}{m_p}\frac{dm_p}{dt} = -\frac{M_C}{\rho_p}R_1 \tag{29}$$

Solution procedure

Given the wall flow rate and the concentrations in the inlet and outlet channels, the intralayer O_2 concentration can be calculated based on Eq. 17 (Danckwerts, 1952) and its boundary conditions, Eqs. 27 and 28. The control volume, including the soot layer and wall, is divided into 40 elements. As shown in Figure 1, the soot layer has a trapezoidal shape when only a quadrant is taken into account because of symmetry. A numerical solution is necessary because of the nonlinearities imposed by the trapezium shape (denoted by the term f_x) and the pressure variation inside the soot layer, which affects the oxygen consumption rate. Because of the deposit depletion, the soot layer is redescretized at every time step in elements of equal mass. An implicit finite-difference method is used, which results in a tridiagonal algebraic system. The solution of the tridiagonal system yields the intralayer O_2 concentrations. The concentration of the first and the last element is used to calculate the O_2 diffusion from the inlet or outlet channel. These diffusion values are then used to calculate the downstream O_2 channel concentrations, which are used as input for the intralayer calculation of the next axial node. This procedure is repeated until the channel exit.

Results and Discussion

Controlled regeneration

The term "controlled" regeneration refers to conditions under which the phenomenon evolves at relatively high flow rate and temperature with moderate-to-low oxygen levels. Such regeneration conditions are typically met when the engine operates at moderate load and speed and the postinjection system is activated. An initial transient mode with a gradual temperature increase is associated with the heat response of the exhaust components placed upstream of the particulate filter. For the present computational study, it will be assumed that the engine operating point and therefore the flow rate and oxygen content remain constant for the regeneration period of 300 s. The flow rate is given the value of 0.03 kg/s, the oxygen content in the exhaust gas is 7%, and the steady-state temperature is 650°C. The filter properties are given in Table 1. The above values, as well as the filter dimensions, are characteristic for a medium-size passenger car diesel engine, regenerating at medium speed with postinjection.

The regeneration will be simulated for different initial soot loadings varying between 4 and 14 g/L. Moreover, each simulation is executed twice, that is, with and without taking into account the oxygen diffusion effects.

Figure 2 presents the computed wall temperatures at different axial positions in the filter channel, assuming a moderate

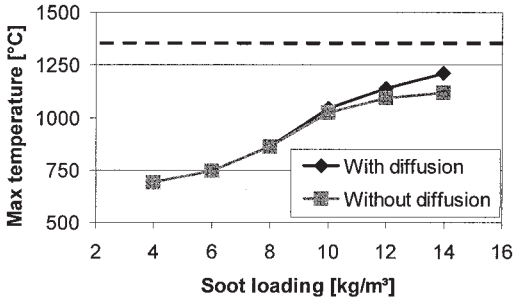

Figure 6. Maximum temperature as function of initial soot mass with and without considering O_2 diffusion effects in controlled regeneration conditions.

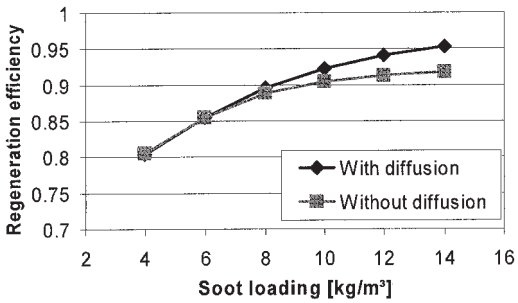

Figure 7. Regeneration efficiency as function of initial soot loading with and without considering O_2 diffusion effects in controlled regeneration conditions.

initial soot loading of 6 kg/m^3. The graph also includes the calculated maximum filter wall temperature. The results in the left graph were obtained with the complete reaction–diffusion model, whereas the diffusion phenomena were neglected in the right graph. It is apparent that the diffusion phenomena do not affect the evolution of filter temperatures in the specific regeneration scenario.

The preceding can also be verified on the basis of the results presented in Figure 3, which shows the computed profiles of O_2 concentration along the filter for the two modeling assumptions. The results correspond to the time of maximum reaction rate, which is around 132 s after start. A constant O_2 concentration along the inlet channel is expected in the case of zero diffusion, which is the case in the right graphs. The O_2 concentration at the exit channel is lower because of the reaction as the flow travels through the soot layer. In the left graphs, which correspond to the combined reaction–diffusion model, the O_2 concentration is decreasing slowly in the inlet and outlet channels together, as a result of the equalizing effect of diffusion. It can be noticed that the O_2 concentration of the outlet channel near the filter exit becomes slightly higher compared to the respective concentration in the inlet channel, implying a "back-diffusion" process from the outlet channel to the soot layer.

The bottom graphs of Figure 3 present the calculated soot layer thickness profiles as well as the local flow rates through the wall for both simulation cases. Because of the relatively low regeneration rate, these profiles are uniform and the differences between the two models are negligible.

Figure 4 presents the simulation results for a regeneration with a higher initial soot loading of 12 kg/m^3. As expected, the temperature increase in the filter is much more pronounced compared to the 6 kg/m^3 loading case. Some minor differences are observed between the left graph (full model) and the right graph (no diffusion model) regarding the maximum filter temperature. Such deviations are normally acceptable for engineering purposes.

The predictions of the two models are quite different in terms of the computed O_2 concentration profiles along the filter, as shown in Figure 5 (132 s after start). The reaction–diffusion model predicts a significant decrease in O_2 concentration in the inlet channel at the rear part of the filter, as a result of diffusion transfer from the bulk flow to the reacting soot layer. Because of the very high local temperatures near the filter exit (Figure 4), the reaction rate is practically limited by oxygen availability. This produces a strong driving force for diffusion from the inlet gas. Moreover, as the flow approaches the rear of the inlet channel, the axial flow rate gradually becomes smaller and smaller as a result of wall flow "losses." This low axial flow rate compared to relatively high oxygen diffusion rate results in an impressively rapid decrease in O_2 concentration in the inlet channel. Such reaction conditions resemble a moving reaction front because the location of this point moves with time according to the time-dependent soot layer profile.

As a result of this diffusion process, the O_2 concentration at the rear of the filter is so low that there is limited oxygen availability for the reaction of the soot. This can be verified by comparing the computed soot layer profiles of the two models. In the right graph the absence of O_2 diffusion results in more effective soot consumption at the rear part of the filter. This is counterbalanced by a somewhat lower soot consumption rate in the middle part of the filter, where oxygen diffusion increases the local reaction rate.

Similar simulations were carried out for various soot loadings ranging from 4 to 14 kg/m^3 with both models. Because the main result of engineering interest is maximum temperature, Figure 6 summarizes the computed maximum temperature results. In the specific controlled regeneration scenario, O_2 diffusion affects the resulting maximum temperature only at

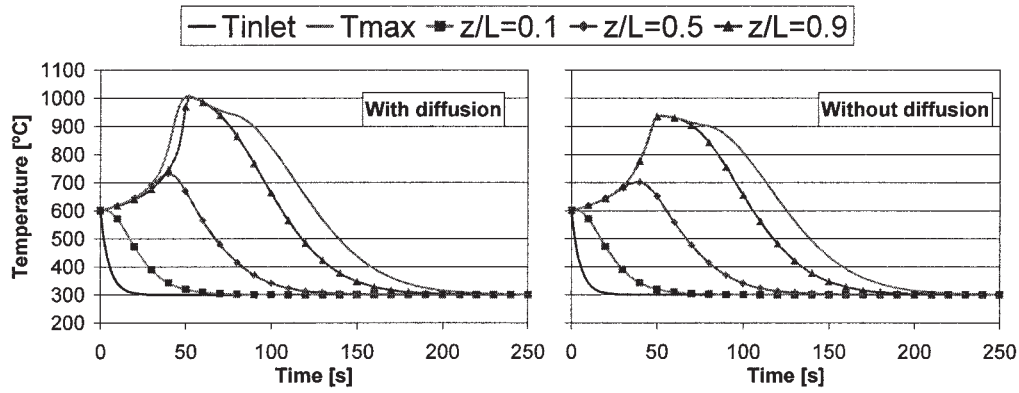

Figure 8. Comparison of temperature predictions during uncontrolled regeneration with and without O_2 diffusion.

Computed temperatures along the filter for 6 kg/m^3 initial soot loading.

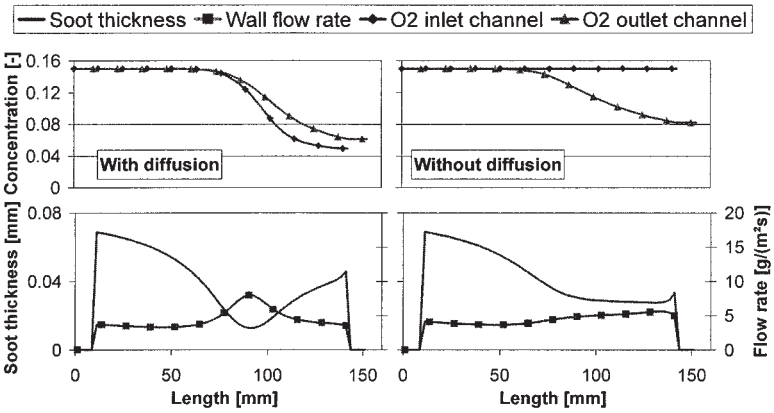

Figure 9. Profiles of O_2 concentration, in the inlet and outlet channels during uncontrolled regeneration.

Conditions: 6 kg/m^3 initial soot mass at $t = 42$ s. Also shown is the wall flow velocity and the soot layer thickness at the same time.

soot loadings higher than 10 kg/m^3. In such cases, neglecting the diffusion effect may result in a minor underprediction of the maximum filter temperature. This is accompanied with a respective difference of the predictions of the regeneration efficiency, which is again underpredicted by the no-diffusion model at high soot loadings, as shown in Figure 7.

Uncontrolled regeneration

Unlike the "controlled" regeneration studied above, "uncontrolled" regenerations typically occur at conditions of low flow rate and high oxygen content and high initial filter temperature. These conditions are usually met when the engine switches to idle mode after a period of high-temperature operation. In the present study, it is assumed that the initial filter temperature is uniform at 600°C. The flow rate is assumed constant at 0.01 kg/s and the oxygen content in the incoming gas equal to 15%. The inlet gas temperature decreases asymptotically from 600 to 300°C with a response time of the order of 20 s. The filter properties are the same as those used in the controlled regeneration study and are given in Table 1. All the above parameter values are typical for a medium-size passenger car diesel engine application.

Figure 8 presents the computed wall temperatures at different axial positions in the filter channel, assuming a moderate initial soot loading of 6 kg/m^3, with and without inclusion of O_2 diffusion effects. Contrary to the controlled regeneration scenario, the diffusion phenomena affect the evolution of filter temperatures, especially with respect to the maximum temperature.

The computed profiles of O_2 concentration along the filter for the two modeling assumptions presented in Figure 9 reveal the O_2 diffusion effects. The results correspond to the time of maximum reaction rate, which is around 42 s after start.

In the left graphs, the O_2 concentration in the inlet channel drops from 15% to about 5% at the rear part, indicating important diffusion effects. These effects have a clear influence on the evolution of the soot layer profile, as well as the wall flow distribution, as shown in the bottom graphs of Figure 9. Because of the O_2 diffusion, the reaction rate in the middle part of the channel is enhanced. It is also interesting to note that the O_2 concentration of the outlet channel near the filter exit is higher compared to the respective concentration in the inlet channel. This concentration difference drives O_2 diffusion back from the outlet channel to the soot layer, thus enhancing the overall reaction rate.

Figure 10 presents the simulation results for an uncontrolled regeneration with a higher initial soot loading of 12 kg/m^3. In this case the differences between the two models are very

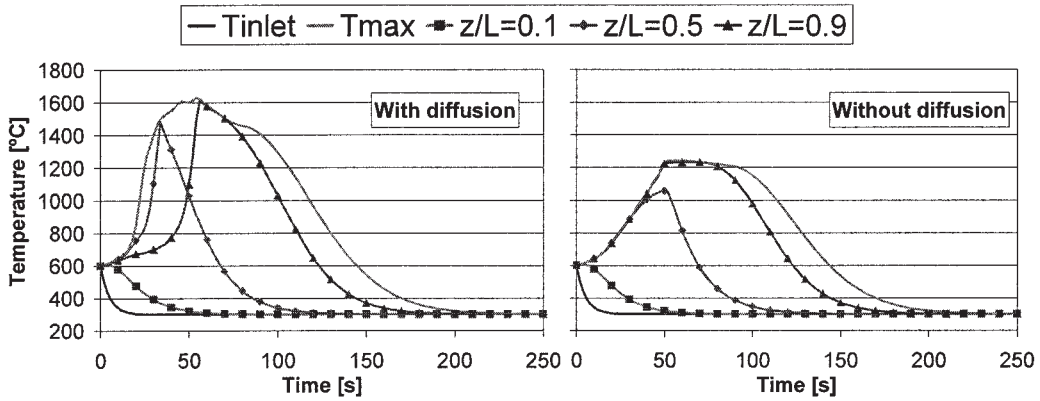

Figure 10. Comparison of temperature predictions during uncontrolled regeneration with and without O_2 diffusion.

Computed temperatures along the filter for 12 kg/m^3 initial soot mass.

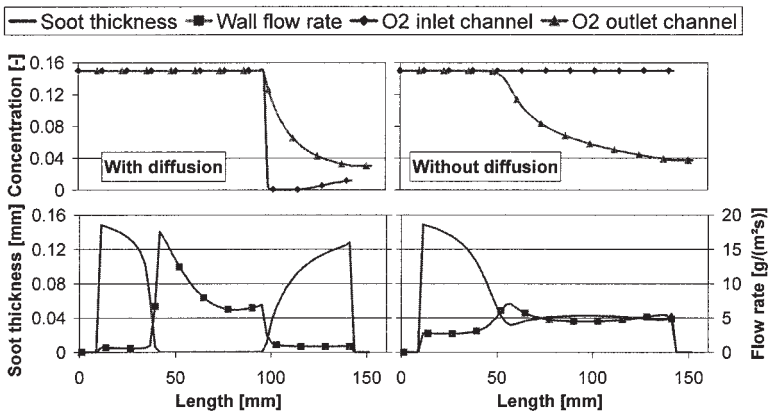

Figure 11. Profiles of O_2 concentration, in the inlet and outlet channels during uncontrolled regeneration.

Conditions: 12 kg/m^3 initial soot mass at $t = 42$ s. Also shown is the wall flow velocity and the soot layer thickness at the same time.

important. In terms of maximum predicted temperature, the difference is of the order of 400°C. Such deviations are critical for model applications concerning the ability of the filter material to withstand severe regeneration conditions.

The computed profiles of O_2 concentration along the filter, presented in Figure 11, are qualitatively similar to those for the case of lower soot loading. Obviously, the O_2 diffusion phenomena are more pronounced and the effects on soot layer evolution and wall-flow distribution very important. The inlet channel O_2 concentration at the specific time drops suddenly from 15% to almost zero at an axial position around 100 mm from the entrance. The concentration again increases slightly toward the rear part of the filter, as a result of diffusion from the outlet back to the inlet channel.

The effect of O_2 diffusion on the evolution of soot layer thickness along the filter channel during regeneration with high soot loading is shown in Figure 12. As shown in the left graph, the diffusion-induced increase of O_2 availability at the middle part of the filter results in a preferential soot consumption compared to the rear part of the filter. This is not the case in the simulation result without O_2 diffusion. The implications in oxygen availability can be also illustrated by examining the O_2 intralayer profiles at different axial points along the filter, as predicted by the two models in Figure 13. The oxygen gradients in the diffusion model imply oxygen transfer from both the inlet and the outlet channels. As expected, close to the filter exit ($z/L = 0.9$), the concentration of oxygen is lower than that expected by the reaction-only model, given that diffusion results in overall increased oxygen consumption up to that axial point.

The maximum temperatures as the function of initial soot loading are shown in Figure 14. The model without O_2 diffusion would predict that the filter temperatures would not exceed the material melting point, which is close to 1350°C, even for initial soot loadings of the order of 14 kg/m^3. On the other hand, the combined model predicts that the regeneration could already be fatal for filter integrity with an initial soot loading of 10 kg/m^3. Finally, the effect of O_2 diffusion in the uncontrolled regeneration efficiency is shown in Figure 15, indicating increased efficiencies as a result of overall higher reaction rates.

Model Validation

A preliminary validation of the reaction–diffusion model is performed based on the experimental data published by Miyari et al. (2001). These experimental data have been obtained during regeneration of a cordierite filter with 200 cpsi (31 cells/cm^2) and 12 mils (0.3048 mm) wall thickness in a propane

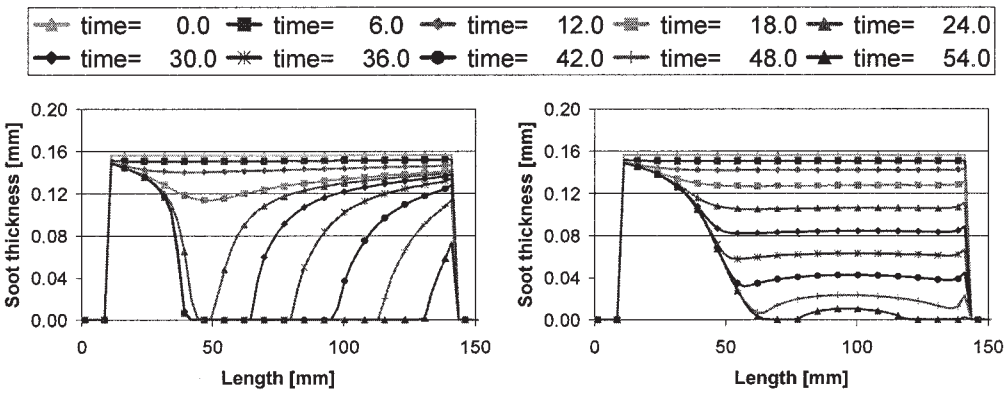

Figure 12. Evolution of soot layer thickness along the filter channel with and without considering O_2 diffusion effects in uncontrolled regeneration.

Conditions: 12 kg/m^3 initial soot loading.

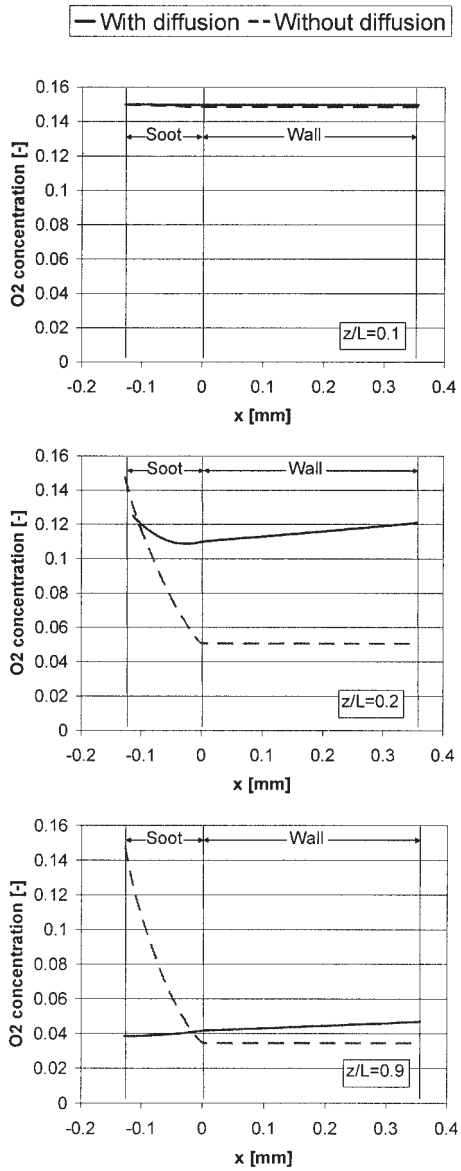

Figure 13. Comparison of intralayer O2 concentration profiles during uncontrolled regeneration.

Conditions: 12 kg/m^3 initial soot mass at $t = 18$ s and $z/L = 0.1$, 0.2, and 0.9.

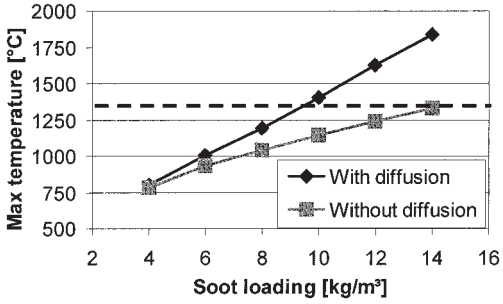

Figure 14. Maximum temperature as function of initial soot mass with and without considering O_2 diffusion effects in uncontrolled regeneration conditions.

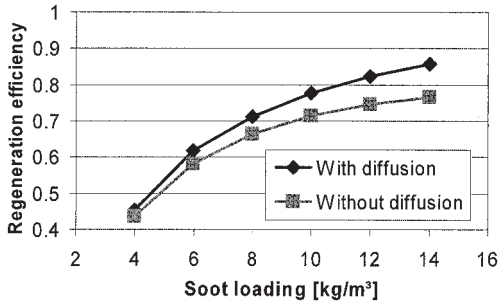

Figure 15. Regeneration efficiency as function of initial soot mass with and without considering O_2 diffusion effects in uncontrolled regeneration conditions.

burner. The regeneration temperature was 600°C and the flow rate 0.014 kg/s. The regenerations were performed with different soot loadings and the temperatures in the filter were recorded in 20 different axial and radial positions in the filter.

To simulate these experiments, it was necessary to use the extended 2-D regeneration model (Haralampous et al., 2003), equipped with the oxygen diffusion submodel presented here. The simulations were carried out twice, with and without diffusion effects. The results are summarized in Figure 16, in terms of the maximum computed filter temperature vs. the respective measurement as a function of initial soot loading.

When diffusion is neglected, the calculated maximum temperature agrees with the measured values for low-to-medium soot loadings up to 8 kg/m^3. At higher soot loadings, which are of interest for filter integrity in uncontrolled regenerations, the discrepancy is critical. On the other hand, inclusion of oxygen diffusion modeling provides a very good agreement with the respective measured data for the complete range of soot loadings. It has to be noted that the model results are quite accurate, even though the reaction scheme for soot reaction is relatively simple. The reaction scheme involves one global oxidation reaction with a simple Arrhenius-type rate expression. Although such a reaction scheme may not be accurate for low-temperature regenerations (Stratakis et al., 2003), where other phenomena possibly interfere (such as hydrocarbon adsorption/desorption), it seems sufficient for the case of uncontrolled

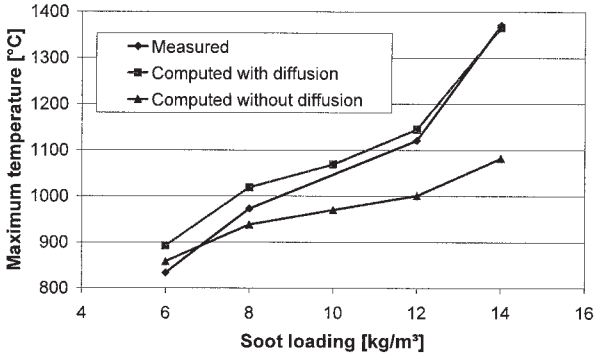

Figure 16. Comparison of experimental and predicted maximum temperatures during regeneration as a function of soot loading.

regeneration conditions where oxygen availability controls the overall rate.

It is interesting to note that the results of this validation exercise are in good agreement with the computational parametric analysis presented in Figure 14, with respect to the range of soot loadings at which oxygen diffusion becomes important.

Conclusions

This article introduced a coupled reaction–diffusion model able to account for O_2 diffusion in the wall-flow honeycomb particulate filter. The diffusion model was incorporated into a previously published single-channel model for the calculation of flow distribution, heat transfer, and soot oxidation reaction. A computational study was carried out aiming at evaluating the importance of O_2 diffusion effects as the function of operating conditions similar to those encountered in the real world. The main conclusions of this computational study can be summarized as follows:

- During controlled regeneration conditions, the effect of O_2 diffusion on the evolution of regeneration is almost negligible for initial soot loadings up to 10 kg/m^3. For higher soot loadings, O_2 diffusion is responsible for slightly higher regeneration rates with respectively higher maximum temperatures and regeneration efficiencies. These small effects can be normally neglected in engineering practice.
- In the uncontrolled regeneration study, the effect of O_2 diffusion was shown to be profoundly important. The "no-diffusion" model underpredicted the maximum temperatures even at soot loadings of the order of 6 kg/m^3. The deviation becomes critical at higher soot loadings, where the material melting point is approached.
- The mechanism of O_2 diffusion becomes important at conditions of reduced local oxygen availability. In these cases, diffusion provides an additional mechanism of sustaining high reaction rates. The soot layer profiles during regeneration are strongly affected by this mechanism, with interesting implications in the wall-flow distribution across the filter channel.
- Modeling is already used as a design tool for modern diesel particulate filter systems. Simulations of uncontrolled regenerations with high soot loadings are used to understand and optimize the regeneration strategies. The present study shows that traditional "no-diffusion" models may seriously underpredict the thermal loading of a filter during such regeneration conditions.
- A preliminary model validation with previously published experimental results was performed. The results are in qualitative and quantitative agreement with the computational parametric analysis.

Notation

A = reaction rate frequency factor
b = geometric parameter Figure 1, m
C_4 = slip flow correction factor, ms(kg mol T)$^{1/2}$
c_m = molecular density, mol/m^3
C_p = specific heat capacity, J/kg·K
cpsi = cell density, cells/in^2
d = hydraulic diameter of clean channel, m
d_i = hydraulic diameter of channel i, m
d_p = mean pore size, m
D = mass diffusivity, m^2/s
E = activation energy, J/mol
f_x = $=b/d$
F = view factor
H = heat transfer per filter volume, W/m^3
h = convection coefficient, W/m^2·K
k_i = mass transfer coefficient of O_2 in channel i, m/s
k_0 = permeability of particulate layer, m^2
k_p = apparent permeability of particulate layer, m^2
k_s = permeability of ceramic substrate, m^2
M = molecular weight, kg/mol
L = filter length, m
m = mass, kg
p = pressure, Pa
$\bar{p}$ = mean pressure of inlet and outlet channels, Pa
p_0 = reference pressure for apparent permeability calculation, Pa
$\Re$ = universal gas constant, J/mol·K
R = reaction rate, mol/(m^{3}s)
S = sum of heat sources, W/m^3
s = specific area of deposit layer, m^{-1}
s_F = filter-specific filtration area, m^{-1}
Sh = Sherwood number
t = time, s
T = temperature, K
v = velocity, m/s
w = particulate layer thickness, m
w_s = channel wall thickness, m
x = space variable perpendicular to wall surface, m
y = mole fraction of species O_2
z = axial distance, m

Greek letters

α = constant in channel pressure drop correlation
α_1 = completeness index of reaction 1
ΔH = reaction heat, J/mol
Δp = backpressure, Pa
ε_p = porosity
λ = thermal conductivity, W/mK
μ = exhaust gas viscosity, kg/ms
ρ = density, kg/m^3
σ = Stefan–Boltzmann constant, W/(m^2 K^4)
τ = tortuosity

Subscripts

$1s$ = inlet channel–soot surface interface ($x = -w$)
$2s$ = outlet channel–wall surface interface ($x = w_s$)
amb = ambient
C = carbon
g = exhaust gas
i = channel index (1 = inlet channel; 2 = outlet channel)
p = particulate layer
s = solid, ceramic substrate
w = wall–outlet channel interface
z = axial direction

Literature Cited

Abthoff, J., H.-D. Schuster, H.-J. Langer, and G. Loose, "The Regenerable Trap Oxidizer—An Emission Control Technique for Diesel Engines," SAE paper no. 850015 (1985).

Aoki, H., K. Asano, K. Kurazono, K. Kobashi, and H. Sami, "Numerical Simulation Model for the Regeneration Process of a Wall-Flow Monolith Diesel Particulate Filter," SAE paper no. 930364 (1993).

Bissett, E. J., "Mathematical Modeling of the Thermal Regeneration of a Wall-Flow Monolith Diesel Particulate Filter," *Chem. Eng. Sci.*, **39**, 1233 (1984).

Bissett, E. J., and F. Shadman, "Thermal Regeneration of Diesel Particulate Monolithic Filters," *AIChE J.*, **31**, 753 (1985).

Cooper, B. J., and J. E. Thoss, "Role of NO in Diesel Particulate Emission Control," SAE paper no. 890404 (1989).

Danckwerts, P. V., "Continuous Flow Systems Distribution of Residence Times," *Chem. Eng. Sci.*, **2**, 1 (1953).

Haralampous, O. A., I. P. Kandylas, G. C. Koltsakis, and Z. C. Samaras, "Diesel Particulate Filter Pressure Drop. Part I: Modeling and Experimental Validation," *Int. J. Engine Res.*, **5**(2), 149 (2004).
Haralampous, O. A., and G. C. Koltsakis, "Intra-Layer Temperature Gradients during Regeneration of Diesel Particulate Filters," *Chem. Eng. Sci.*, **57**, 2345 (2002).
Haralampous, O. A., G. C. Koltsakis, and Z. C. Samaras, "Partial Regenerations in Diesel Particulate Filters," SAE paper no. 2003-01-1881 (2003).
Hayes, R. E., S. T. Kolaczkowki, P. K. Li, and C. S. Awdry, "Evaluating the Effective Diffusivity of Methane in the Washcoat of a Honeycomb Monolith," *Appl. Catal. B: Environ*., **25**, 93 (2000).
Howitt, J. S., and M. R. Montierth, "Cellular Ceramic Diesel Particulate Filter," SAE paper no. 810114 (1981).
Johnson, V. T., "Diesel Emission Control in Review—The Last 12 Months," SAE paper no. 2003-01-0039 (2003).
Kolaczkowski, S. T., "Measurement of Effective Diffusivity in Catalyst-Coated Monoliths," *Catal. Today*, **83**, 85 (2003).
Koltsakis, G. C., and A. M. Stamatelos, "Modes of Catalytic Regeneration in Diesel Particulate Filters," *Ind. Eng. Chem. Res.*, **36**, 4255 (1997).
Konstandopoulos, A. G., M. Kostoglou, and P. Housiada, "Spatial Non-Uniformities in Diesel Particulate Trap Regeneration," SAE paper no. 2001-01-0908 (2001).
Miyairi, Y., S. Miwa, F. Abe, Z. Xu, and Y. Nakasuji, "Numerical Study on Forced Regeneration of Wall-Flow Diesel Particulate Filters," SAE paper no. 2001-01-0912 (2001).
Pontikakis, G., A. Stamatelos, K. Bakasis, and N. Aravas, "3-D Catalytic Regeneration and Stress Modeling of Diesel Particulate Filters by ABAQUS FEM Software," *SAE 2002 Trans.*, SAE paper 2002-01-1017 [*J. Fuels & Lubricants*, 458 (2002)].
Pulkrabek, W. W., and W. E. Ibele, "The Effect of Temperature on the Permeability of a Porous Material," *Int. J. Heat & Mass Transfer*, **30**(6), 1103 (1987).
Salvat, O., P. Marez, and G. Belot, "Passenger Car Serial Application of a Particulate filter System on a Common Rail Direct Injection Diesel Engine," SAE paper no. 2000-01-0473 (2000).
Stratakis, G. A., G. S. Konstantas, and A. M. Stamatelos, "Experimental Investigation of the Role of Soot VOF in the Regeneration of Diesel Filters," *Proc. Inst. Mech. Eng. D: J. Automobile Eng.*, **217**, 307 (2003).
Suresh, A., J. H. Johnson, S. T. Bagley, and D. G. Leddy, "A Study of the Effect of a Catalyzed Particulate Filter on the Emissions from a Heavy-Duty Diesel Engine with EGR," SAE paper no. 2001-01-0910 (2001).

Manuscript received Sep. 23, 2003, and revision received Dec. 4, 2003.